NON-HYDROSTATIC ADIABATIC KERNEL FOR HIRLAM
Part IV
Semi–implicit semi–Lagrangian scheme

Rein Rõõm, Aarne Männik, Andres Luhamaa
Tartu University, Estonia
Rein.Room@ut.ee, Aarne.Mannik@ut.ee, Andres.Luhamaa@ut.ee

1 Introduction

The adiabatic kernel of the nonhydrostatic (**NH**) HIRLAM with the semi-implicit semi-Lagrangian (**SISL**) integration scheme is presented in this paper. Our investigation continues the work, initiated in the *Parts* $I - III$ (Rõõm 2001, Männik and Rõõm 2001, Rõõm and Männik 2002), where the fundamentals of NH atmospheric dynamics in pressure–related coordinates were presented, and, on that basis, the NH explicit-Eulerian and semi-implicit (**SI**) Eulerian versions of HIRLAM were developed.

SISL has become the popular integration scheme in all advanced weather forecast systems in last two decades. The main advantage of SISL (in comparison with competing schemes like the SI Eulerian scheme or time-split-explicit scheme) is the significantly enhanced overall computational efficiency, which is achieved through substantial gain in numerical stability at the increased time step.

The SISL-ideology to integrate the HS primitive equations numerically was first proposed by Robert (1981, 1982), who proceeded from an earlier positive experience with the SI Eulerian scheme [1]. A baroclinic, multi-level, HS primitive-equation, three-time-level SISL model was first presented by Robert, Yee and Richie (1985). An alternative approach with two-time-level scheme was developed by Temperton and Staniforth (1987). In operational forecast, SISL has implemented in the middle of the last century nineties. At ECMWF the two-time-level SISL was operationally launched in 1995 (Ritchie et al 1995). For HIRLAM, the two-time-level SISL scheme was introduced by McDonald and Haugen (1992), and further developed by McDonald (1995). Finally, McDonald (1998, 1999) carried out a further extensive investigation to improve the departure point evaluation. Developed by him non-iterative departure point calculation algorithm is currently in use at the operational HIRLAM.

The first NH, fully compressible (i.e. making use of complete, non-simplified set of dynamic equations) SISL was proposed already in 1990 (Tanguay, Robert and Laprise, 1990), but an acute actuality for operational forecasting it has gained in last years in connection with model transition into NH-resolution domain.

[1] Three time level SI Eulerian scheme was proposed by Robert (1969); the first baroclinic multi-level SI Eulerian scheme for HS primitive equations was described in (Robert, Henderson, Thurnbull 1972).

Adiabatic dynamics, applied in current NH SISL scheme, is the *White model* (White 1989), which represents a simplified version of complete NH pressure-coordinate equations. Roughly speaking, White model is the simplest generalization of the hydrostatic, primitive-equation, pressure-coordinate dynamics which incorporates the vertical momentum equation and takes vertical acceleration into consideration. This closeness to HS model makes implementation of NH dynamics into existing HS environment of HIRLAM rather straightforward. The White model derivation from general elastic pressure-coordinate equations with description of main qualities is presented in detail in (Rõõm 2001). As comparison with the exact analytical solutions (Rõõm and Männik 1989), and with the 'full' elastic model (French NH Aladin) on the non-linear test flows have demonstrated (Männik 2003), there is no sensible difference between 'exact dynamics' and White model results. The White model has been already applied with success in heretofore developed three-time-level, explicit-Eulerian (Männik and Rõõm 2001), and SI Eulerian (Rõõm, Männik 2002, Männik, Rõõm, Luhamaa 2003) schemes. In those models, an additional approximation of the surface pressure adjustment was introduced, which gave reason to call that approach 'anelastic pressure coordinate model', as the acoustic travelling waves were completely eliminated from dynamics[2]. In the current NH SISL model, we will restore the non-adjusted pressure treatment of the original White model, which, however, could be still called 'semi-anelastic' because it lacks internal acoustic mode due to non-divergence of three-dimensional (**3D**) velocity in pressure-coordinates.

The most plain reason for discarding with surface pressure adjustment was that the implicit treatment of linear development in SISL does not require such an approximation anymore. Adjustment is actually essential in the explicit-Eulerian scheme where it yields significant growth of computational efficiency, expressed in the increase of achievable time step, while in the implicit schemes, the time-step rise is achieved by other, independent means (just by implicit treatment of linear forces). More considerable reason, however, was the experimentally established fact that dynamics with the adjust-

[2]By the way, using of terminology 'anelastic' served us a disservice, as it was often confused with anelasticity interpretations in shallow convection (constant reference density $\rho = const$) or deep convection (fixed reference density $\rho = \rho_0(z)$) models. Actually, with the term 'anelastic' we tried just to underline that model lacks acoustic waves – exactly like the HS primitive-equation model does, likewise being anelastic with respect to the internal (vertically propagating) sound waves.

ment approximation may lead to a discontinuity of nonhydrostatic geopotential field at surface, when the time step becomes over one critical[3]. Finally, the non-adjusted, non-simplified model is simpler to deal with in the formal plane. Thus, the non-adjusted surface pressure evolution is restored in this paper.

Another mayor novelty consist in preceding modifications of geopotential and surface pressure treatment. The neutral reference states are subtracted from geopotential and surface pressure in the very beginning, in continuous equations already, confining the treatment to evolution of geopotential and pressure fluctuations. Ideologically this approach is similar to 'Eulerian advection of orography' method by Richie and Tanguay (1996). However, in the current treatment, the modification is applied before any discretization, which refers to generality of such an approach. The aim of the modification is elimination of large, dynamically passive fields, otherwise just being a source of additional noise in the numerical scheme.

The last model-specific modification, yet no the least one, is the application of height-dependent reference temperature $T^0(p)$ together with the accompanying height-dependent reference-state Brunt-Väisälä frequency $N(p)$, both giving some rise to stability, as the non-linear residuals are minimized in the vertical development equations.

The NH model altogether aims to be an organic and straightforward extension of the HS SISL core to NH resolutions. Thus, except the necessary modifications of dynamic equations, almost all the numerical scheme is maintained from the HS parent. This includes the use of the two-time-level time-stepping with the complete maintenance of the departure point calculation procedures (McDonald 1998, 1999) and interpolation routines. And, of course, the diabatic counterpart, consisting the so-called 'physics', which is not concern of adiabatic core development, is maintained untouched, and is overtaken from HS model without any change and modification.

[3]Critical time step in the sense of the Courant-Fiedrichs-Lewy stability criterion.

2 Basic equations

Concerning the basic equations, as well as notations, this paper is a direct successor of the papers (Rõõm. 2001, Männik and Rõõm, 2001, and Rõõm, Männik 2002), and keeps to the general HIRLAM standards (Manual 1996, Manual 2004). However, for reader's ease the basic definitions of constants, variables, fields and operators are summarised in Appendix 1.

2.1 Primary modifications

In the continuous pressure-coordinate case, the basic equations of the White Model are presented and comprehensively discussed in our former paper (Rõõm, 2001, equations (3.2)). Two substantial differences with those equations in current case are, first, the use of full, evolutional surface pressure equation, and, second, modified handling of geopotential and surface pressure.

2.1.1 Surface pressure equation

The departure point equation for surface pressure is the continuity equation in η–coordinates

$$\frac{\partial m}{\partial t} + \nabla \cdot (m\mathbf{v}) + \frac{\partial m\dot{\eta}}{\partial \eta} = 0,$$

which, in the vertically discrete case ($m = \Delta_k p/\Delta\eta$), can be presented (after omitting of constant $\Delta\eta$ everywhere)

$$\frac{\mathrm{d}_k^h \Delta_k p}{\mathrm{d}t} + \Delta_k p D_k + \Delta_k (m\dot{\eta}) = 0, \tag{2.1}$$

where

$$D_k = \nabla\cdot \mathbf{v}_k, \qquad \frac{\mathrm{d}_k^h}{\mathrm{d}t} = \frac{\partial}{\partial t} + \mathbf{v}_k\nabla.$$

Note that horizontal divergence in this definition is evaluated on fixed η-surface and for spherical geometry with fixed curvature, equal to the mean radius of Earth. As $p_{k+1/2} = A_{k+1/2} + B_{k+1/2}p_s$, one has $\mathrm{d}_k^h(\Delta_k p)/\mathrm{d}t = \Delta_k B \mathrm{d}_k^h p_s/\mathrm{d}t$ and, after dividing by p_s, equation (2.1) presents

$$\Delta_k B \frac{\mathrm{d}_k^h \ln p_s}{\mathrm{d}t} + \frac{\Delta_k p}{p_s} D_k + \frac{\Delta_k (m\dot{\eta})}{p_s} = 0.$$

From this equation we will subtract the identity

$$\Delta_k B \left(\frac{\mathrm{d}_k^h \ln \hat{p}_s}{\mathrm{d}t} - \mathbf{v}_k \cdot \nabla(\ln \hat{p}_s) \right) = 0, \qquad (*)$$

where reference surface pressure $\hat{p}_s$ is defined as

$$\hat{p}_s = p_s^0 \exp\left(-g \int_o^h \frac{dz}{R^0 T^0(z)} \right) \qquad (2.2)$$

for the given orography (surface elevation) h, mean sea level pressure p_s^0, and appropriate[4] reference temperature $T^0(z)$. As the result of the subtraction we obtain a prognostic equation

$$\Delta_k B \frac{\mathrm{d}_k^h \chi}{\mathrm{d}t} + \frac{\Delta_k p}{p_s} D_k + \frac{\Delta_k (m\dot{\eta})}{p_s} + \Delta_k B \mathbf{v}_k \cdot \nabla(\ln \hat{p}_s) = 0 \qquad (2.3)$$

for logarithmic surface pressure deviation

$$\chi = \ln(p_s / \hat{p}_s) \qquad (2.4)$$

on level k. Equation (2.3) is a partial equation with the weight $\Delta_k B$, describing the contribution of the layer k to the overall (total) change of surface pressure. To get the total evolution, partial equations (2.3) should be summed up over all layers. However, it is reasonable to postpone this summation until arriving at the final Lagrangian time-stepping formulae. The described subtraction of equation (*) means factually introduction of the 'Eulerian advection of orography', first applied in Lagrangian scheme by Richie and Tanguay (1996). The Eulerian advection of the (mean) orography is presented in Eq. (2.3) by term $\mathbf{v}_k \cdot \nabla(\ln \hat{p}_s)$.

Despite of unusual (non-traditional) appearance, (partial) surface pressure equation (2.3) is rather convenient and useful for application, as the logarithmic pressure fluctuation (2.4) is the prime quantity, describing the surface pressure contribution to the fluctuations of hydrostatic pressure (see below).

2.1.2 Diagnostic relations for omega- and eta-velocities

The SISL scheme requires diagnostic evaluation of ω and $\dot{\eta}$ on the past time levels. For $m\dot{\eta}$ the continuity equation (2.1) can be applied (employed) to

[4]Horizontal mean over the domain of integration, as an example.

get a recurrence

$$(m\dot{\eta})_{k+1/2} = (m\dot{\eta})_{k-1/2} - \nabla \cdot (\mathbf{v}\Delta p)_k - \Delta_k B \frac{\partial p_s}{\partial t}, \tag{2.6}$$

where $\partial p_s/\partial t$ is (a consequence of (2.1) after use of Eulerian representation and summation over all levels)

$$\frac{\partial p_s}{\partial t} = -\nabla \cdot \sum_{k=1}^{klev} \mathbf{v}_k \Delta_k p, \tag{2.5}$$

Diagnostic equation for ω follows, if one applies Lagrangian time derivation d/dt to pressure expression in eta–coordinates $p = A(\eta) + B(\eta)p_s$ and applies the result on the discrete eta-level $k + 1/2$:

$$\omega_{k+1/2} = (m\dot{\eta})_{k+1/2} + B_{k+1/2}\left(\overline{\mathbf{v}}^{\eta}_{k+1/2} \cdot \nabla p_s + \frac{\partial p_s}{\partial t}\right). \tag{2.7}$$

This is an diagnostic formula for ω, if considered together with (2.5) and (2.6).

2.1.3 Geopotential

Geopotential for general NH model in pressure coordinates is discussed in (Rõõm, 2001). In this paper, we will use division of the full geopotential to the hydrostatic component φ^s and to the non-hydrostatic supplementation ϕ (see *ibid*, formula (2.5.2a))

$$\Phi = \varphi^s + \phi.$$

Note that such separation is natural for a model with the non-adjusted (full) surface pressure treatment, differently from the adjusted model with geopotential separation to the baric and thermal components (*ibid*, formula (2.5.3a)).

In continuous pressure-coordinate presentation the hydrostatic component is conventional:

$$\varphi^s = gh + \int_p^{p_s} RTd(\ln p').$$

It is useful (as a numerical noise reduction remedy) to subtract from this geopotential a neutral background geopotential

$$\hat{\varphi} = gh + \int_p^{\hat{p}_s} R^0 T^0(p') d(\ln p'),$$

where $\hat{p}_s$ is the reference surface pressure, R^0 is the gas constant for dry air, and $T^0(p)$ is the reference temperature distribution. If $\hat{p}_s$ is chosen to satisfy the condition (equivalent to the barometric formula (2.2))

$$\int_{\hat{p}_s}^{p_s^0} R^0 T^0(p') d(\ln p') = gh(x, y),$$

then

$$(\nabla \hat{\varphi})_p = 0,$$

i.e., the horizontal pressure-force from geopotential is zero and this geopotential may be safely subtracted from ϕ^* without dread of actual forcing loose or virtual forcing creation.

Using alternative presentation

$$\hat{\varphi} = gh + \int_p^{p_s} R^0 T^0(p') d(\ln p') - \int_{\hat{p}_s}^{p_s} R^0 T^0(p') d(\ln p')$$

$$= gh + \int_p^{p_s} R^0 T^0(p') d(\ln p') - R^0 T^0(\hat{p}_s)\chi.$$

we arrive at expression for fluctuative HS geopotential

$$\varphi = \varphi^* - \hat{\varphi} = R^0 T^0(\hat{p}_s)\chi + \int_p^{p_s} (RT)' d(\ln p'), \tag{2.8}$$

where

$$(RT)' = RT - R^0 T^0(p).$$

The derived formula (2.8) presents HS geopotential fluctuation, which is essential for dynamics, while causing the real forces in the system. This fluctuative part is small, when measured in units $R^0 T^0$: the amplitude of χ is about 1/100, whereas the amplitude of the integral term in units $R^0 T^0$ is about 1/10.

In hybrid coordinates the formula for φ reads

$$\varphi = R^0 T^0(\hat{p}_s)\chi + \int_\eta^1 (RT)' \frac{\partial \ln p}{\partial \eta'} d\eta',$$

and in the discrete approximation we obtain

$$\varphi_k = R^0 T^0(\hat{p}_s)\chi + \Gamma_k (RT)', \tag{2.9}$$

where

$$\Gamma_k \xi = \sum_{j=k+1}^{klev} \alpha_j \xi_j + \frac{1}{2}\alpha_k \xi_k.$$

$$\alpha_k = 2\frac{p_{k+1/2} - p_{k-1/2}}{p_{k+1/2} + p_{k-1/2}} = \frac{\Delta_k p}{\overline{p}_k^\eta}.$$

Respectively, in momentum equations, the complete geopotential Φ will be replaced with the fluctuative geopotential, consisting of HS and NH parts

$$\Phi' = \varphi + \phi.$$

The non-hydrostatic component ϕ is caused by system departure from HS equilibrium. In detail its main features are discussed in (Rõõm, 2001). Essential for current treatment is the lower boundary condition

$$\phi|_{p_s} = 0, \tag{2.10}$$

which represents the Dirichlet' homogeneous BC (while treated in conjunction with the Laplace equation for ϕ as demonstrated further).

2.2 Initial equations

The equations of motion and thermodynamics, in vertically discrete hybrid coordinate, Lagrangian presentation, yet in continuous time, and with modifications for geopotential and surface pressure equation introduced in the previous section, are as follow:

Vertical momentum equation

$$\frac{\mathrm{d}_{k+1/2}\omega}{\mathrm{d}t} = -(W\Delta\phi)_{k+1/2} + (a^0_\omega)_{k+1/2}, \tag{2.11a}$$

Horizontal momentum (wind) equation

$$\frac{\mathrm{d}_k\mathbf{v}}{\mathrm{d}t} = -\hat{\mathbf{G}}_k(\phi+\varphi) - \mathbf{f}\times\mathbf{v}_k + \mathbf{A}_{\mathbf{v}k}\ ; \tag{2.11b}$$

Temperature equation (for fluctuative part of temperature)

$$\frac{\mathrm{d}_k T'}{\mathrm{d}t} = S_k\overline{\omega}^\eta_k + (A_T)_k; \tag{2.11c}$$

Surface pressure k-level partial equation

$$\Delta_k B\frac{\mathrm{d}^h_k\chi}{\mathrm{d}t} = -\frac{\Delta_k p}{p_s}D_k - \frac{\Delta_k(m\dot\eta)}{p_s} - \Delta_k B\mathbf{v}_k\cdot\nabla(\ln\hat p_s). \tag{2.11d}$$

Continuity equation (condition of non-divergence of 3D velocity)

$$\hat{\mathbf{G}}^+_k\cdot\mathbf{v} + \frac{\Delta_k\omega}{\Delta_k p} = 0\ . \tag{2.11e}$$

The coefficients in these equations are

$$W_{k+1/2} = \left(\frac{(gp)^2}{\overline{(RT)^2\Delta p}^\eta}\right)_{k+1/2}, \qquad S_k = \left(\frac{\varkappa T}{\overline{p}^\eta}\right)_k - \frac{\Delta_k T^0}{\Delta_k p} \tag{2.12a}$$

(where T^0 depends via $p_k(x,y)$ on horizontal coordinates x, y),

$$(a^0_\omega)_{k+1/2} = \omega_{k+1/2}\left(\frac{c_v\omega}{c_p p} - \frac{A_T}{T} - \frac{\mathrm{d}\ln R}{\mathrm{d}t}\right)_{k+1/2} + A_\omega, \tag{2.12b}$$

Terms $\mathbf{A}_\mathbf{v}$, A_T and A_ω are general notation for diabatic forcing and spectral smoothing.

3 Semi-implicit semi-Lagrangian discrete approximation of dynamics

3.1 Separation of linear main terms and nonlinear perturbations in equations

Division of forcing in equations to the main and perturbation parts is based on the treatment of the linear part of equations as a main forcing and supplementation of these linear terms to the full forcing by nonlinear residuals as the perturbation. The linear terms are thereafter treated implicitly, whereas the nonlinear perturbations are considered in the explicit manner.

The linear part corresponds to a fixed, horizontally homogeneous reference state, characterized by the temperature $T^0(p)$ and uniform ground surface with constant surface pressure p_s^0.

Departure of temperature from the reference state, and of the surface pressure from the uniform, constant value, are responsible for the perturbation terms.

The partition in equation (2.11a) takes advantage of presentation

$$W_{k+1/2} = W^0_{k+1/2} + W'_{k+1/2}, \qquad W^0_{k+1/2} = \left[\frac{(gp^0)^2}{(R^0T^0(p^0))^2\overline{\Delta p^0}^{\eta}}\right]_{k+1/2}$$

with W defined in (2.12a). Thus, W^0 is the main part and W' is the nonlinear perturbation of W, which is evaluated at every instant as

$$W'_{k+1/2} = W_{k+1/2} - W^0_{k+1/2}.$$

For $T^0(p)$, the mean actual temperature over the area at the fixed pressure (the p-mean temperature) is assumed. The reference pressure $p^0_{k+1/2}$ corresponds to the even ground with constant pressure p_s^0:

$$p^0_{k+1/2} = A_{k+1/2} + B_{k+1/2}p_s^0 = \eta_{k+1/2}p_s^0.$$

In application, the mean (averaged over area of integration at every instant) surface pressure is used for p_s^0.

Division for coefficient S in equation (2.11c) is

$$S_k = S^0_k + S'_k, \quad \text{where} \quad S^0_k = \frac{\varkappa^0 T^0(p^0_k)}{p^0_k} - \frac{\Delta_k T^0(p^0)}{\Delta_k p^0}.$$

Horizontal p-gradient $\hat{\mathbf{G}}(\phi+\varphi)$ in (2.11b) divides

$$\hat{\mathbf{G}}_k(\phi+\varphi) = \overline{\nabla}(\phi+\varphi^0) + [\hat{\mathbf{G}}_k(\phi+\varphi)]'$$

where the 'plain' gradient $\overline{\nabla}$ is the main part of $\hat{\mathbf{G}}$, while the main part of hydrostatic geopotential is

$$\varphi_k^0 = C^2\chi + R^0\Gamma_k^0(T)', \tag{3.1}$$

where

$$C^2 = R^0T^0(p_s^0),$$

$$\Gamma_k^0\xi = \sum_{j=k+1}^{klev} \alpha_j^0\xi_j + \frac{1}{2}\alpha_k^0\xi_k.$$

$$\alpha_k^0 = 2\frac{p_{k+1/2}^0 - p_{k-1/2}^0}{p_{k+1/2}^0 + p_{k-1/2}^0} = \frac{\Delta p_k^0}{\overline{p^0}_k^{\eta}}.$$

(The nonhydrostatic geopotential like other prime dynamic fields does not need any separation, yet HS geopotential, which is a function of T' and χ with coefficients, depending on pressure, is subject to separation). The perturbation part of horizontal pressure forcing is presented without any simplification as the difference between full and linear pressure forces

$$[\hat{\mathbf{G}}_k(\phi+\varphi)]' = \hat{\mathbf{G}}_k(\phi+\varphi) - \overline{\nabla}(\phi+\varphi^0).$$

As a result, equations (2) present

$$i,j,k{+}1/2: \qquad \frac{\mathrm{d}\omega}{\mathrm{d}t} = -W^0\Delta\phi + a_\omega, \tag{3.2a}$$

$$i{+}1/2,j,k: \qquad \frac{\mathrm{d}u}{\mathrm{d}t} = -\overline{\nabla}_x(\phi+\varphi^0) + a_u\ , \tag{3.2b}$$

$$i,j{+}1/2,k: \qquad \frac{\mathrm{d}v}{\mathrm{d}t} = -\overline{\nabla}_y(\phi+\varphi^0) + a_v\ , \tag{3.2c}$$

$$i,j,k: \qquad \frac{\mathrm{d}T'}{\mathrm{d}t} = S^0\overline{\omega}^{\eta} + a_T, \tag{3.2d}$$

$$i,j,k: \qquad \Delta B\frac{\mathrm{d}^h\chi}{\mathrm{d}t} = -\frac{\Delta p^0}{p_s^0}D^0 - a_\chi, \tag{3.2e}$$

$$i,j,k: \qquad D_k^0 + \frac{\Delta\omega}{\Delta p^0} + a_D = 0\ , \qquad (3.2f)$$

where D^0 is the 2D divergence in plane geometry

$$D_k^0 = \overline{\nabla}_x u + \overline{\nabla}_y v.$$

The nonlinear terms in these presentations are

$$a_\omega = a_\omega^0 - W'\Delta\phi, \qquad a_T = S'\overline{\omega}^\eta + A_T,$$

$$a_u = -\left[\hat{\mathbf{G}}_x(\phi+\varphi) - \overline{\nabla}_x(\phi+\varphi^0)\right] + fv + A_u\ ,$$

$$a_v = -\left[\hat{\mathbf{G}}_y(\phi+\varphi) - \overline{\nabla}_y(\phi+\varphi^0)\right] - fu + A_v\ ,$$

$$a_\chi = \frac{\Delta p}{p_s}D - \frac{\Delta p^0}{p_s^0}D^0 + \frac{\Delta(m\dot{\eta})}{p_s} + \Delta B\mathbf{v}\cdot\nabla(\ln\hat{p}_s),$$

$$a_D = \left(\hat{\mathbf{G}}_x^+ u + \hat{\mathbf{G}}_y^+ v + \frac{\Delta\omega}{\Delta p}\right) - \left(D^0 + \frac{\Delta\omega}{\Delta p^0}\right).$$

3.2 SISL approximation

Equations (3.2) are still in continuous time. Their further modification is based on the application to them of the two-time-level, semi-implicit, semi-Lagrangian scheme (McDonald and Haugen 1992, 1993, McDonald 1995, 1998, 1999).

The SISL ideology is concisely as follows. Let us present equations (3.a) - (3.2f) in general notation as

$$\frac{\mathrm{d}\psi}{\mathrm{d}t} = F + a,$$

with the linear main part F and perturbation part a. The SISL approximation of this equation is

$$\frac{\psi^{t+\Delta t} - \psi_*^t}{\Delta t} = \frac{1-\varepsilon}{2}F_*^t + \frac{1+\varepsilon}{2}F^{t+\Delta t} + \frac{1-\varepsilon}{2}a_*^{t+\Delta t/2} + \frac{1+\varepsilon}{2}a^{t+\Delta t/2}. \quad (3.3)$$

According to this expression, an air particle arrives in the given location (witch is usually a grid-point) with coordinate $\mathbf{x} = \mathbf{x}(t+\Delta t)$ at the moment

$t + \Delta t$ from the departure point $\mathbf{x}_* = \mathbf{x}_*(t)$, where it was at time t. The values of the fields ψ, F in the departure point and in the final point are ψ_*^t, F_*^t, $\psi^{t+\Delta t}$, $F^{t+\Delta t}$, respectively. Expression on the left side of (3.3) is the finite-difference Lagrangian approximation for material derivative of ψ. Forces on the right side are weighted averages of those of the continuous model. The main linear term F is the weighted average of its departure value in the initial moment and final value at the arrival point. This use of the final value $F^{t+\Delta t}$ makes the scheme implicit with respect to the linear force. The nonlinear term a is also a weighted average between its departure- and arrival-point values, but in this case the averaging is carried out for intermediate time $t + \Delta t/2$ and thus, this term is approximated explicitly. The small parameter ε is introduced to increase the weight of the arrival point in forcing formation. Typically the value of this parameter is in the interval $0 < \varepsilon \leq 0.1$.

Central issues of the application of described approach are the departure point $\mathbf{x}_*$ evaluation, intermediate field $a^{t+\Delta t/2}$ calculation, and interpolation of fields F^t and $a^{t+\Delta t/2}$ from grid-points to the departure point locations.

For calculation of a at intermediate time level the Adams-Bashford extrapolation scheme is used:

$$a^{t+\Delta t/2} = 1.5a^t - 0.5a^{t-\Delta t}.$$

The departure point evaluation is based on the non-linear equation

$$\mathbf{x} - \mathbf{x}_* = \Delta t \mathbf{v}^{t+\Delta t/2}[(\mathbf{x} + \mathbf{x}_*)/2].$$

Initially, this equation was solved iteratively (McDonald and Haugen 1993, McDonald 1995). Later, McDonald introduced an efficient non-iterative algorithm (McDonald 1998, 1999, Manual 2002) (representing a generalization of the approach by Tempertone and Staniforth, 1987)

$$\mathbf{x} - \mathbf{x}_* = \Delta t \hat{\mathbf{V}},$$

$$\hat{\mathbf{V}} = a\mathbf{v}_{\mathbf{x}}^t + c\mathbf{v}_{\mathbf{x}-\mathbf{v}_{\mathbf{x}}^t\Delta t}^t + e\mathbf{v}_{\mathbf{x}-2\mathbf{v}_{\mathbf{x}}^t\Delta t}^t + b\mathbf{v}_{\mathbf{x}}^{t-\Delta t} + d\mathbf{v}_{\mathbf{x}-\mathbf{v}_{\mathbf{x}}^t\Delta t}^{t-\Delta t} + f\mathbf{v}_{\mathbf{x}-2\mathbf{v}_{\mathbf{x}}^t\Delta t}^{t-\Delta t}$$

with constants

$$a = -0.25, \quad b = 0, \quad c = 1.50, \quad d = 0.5, \quad e = 0.25, \quad f = -1.0.$$

The great advantage of the described approach is that the departure point calculation and interpolation issues do not depend on physical details of

the modelled system. Thus, all the described trajectory calculus, initially developed for HS dynamics, is applicable without changes also in the NH model.

Solution of equation (3.3) with respect to fields at time level $t + \Delta t$ yields

$$\psi^{t+\Delta t} - \Delta t_+ F^{t+\Delta t} = \hat{\psi}, \tag{3.4}$$

where

$$\hat{\psi} = \left(\psi^t + \Delta t_- F^t + \Delta t_- a^{t+\Delta t/2}\right)_* + \Delta t_+ a^{t+\Delta t/2}$$

and

$$\Delta t_\pm = \frac{1 \pm \varepsilon}{2} \Delta t,$$

The general formula (3.4) for evaluation of final fields at the arrival point is the basis for further transformation of equations (3.2).

3.3 One-step integrals of SISL-model equations

Application of formula (3.4) to equations (3.2a) - (3.2e) yields one-time-step-integrals

$$i, j, k{+}1/2: \qquad \omega^{t+\Delta t} + \Delta t_+ W^0 \Delta\phi^{t+\Delta t} = \hat{\omega}\ , \tag{3.5a}$$

$$i{+}1/2, j, k: \qquad u^{t+\Delta t} + \Delta t_+ \overline{\nabla}_x \left(\phi + \varphi^0\right)^{t+\Delta t} = \tilde{u}, \tag{3.5b}$$

$$i, j{+}1/2, k: \qquad v^{t+\Delta t} + \Delta t_+ \overline{\nabla}_y \left(\phi + \varphi^0\right)^{t+\Delta t} = \tilde{v}\ , \tag{3.5c}$$

$$i, j, k: \qquad T'^{t+\Delta t} - \Delta t_+ S^0 (\overline{\omega}^\eta)^{t+\Delta t} = \hat{T}\ , \tag{3.5d}$$

$$i, j: \qquad \chi^{t+\Delta t} + \Delta t_+ \sum_{k=1}^{klev} \frac{\Delta p_k^0}{p_s^0} (D_k^0)^{t+\Delta t} = \tilde{\chi}, \tag{3.5e}$$

while the continuity equation (3.2f) gives

$$i, j, k: \qquad \left(D^0 + \frac{\Delta\omega}{\Delta p^0}\right)^{t+\Delta t} = -\hat{\mathcal{D}}, \tag{3.5f}$$

The partial surface pressure equations (3.2e) are eventually summed up to get the relationship (3.5e).

The quest fields/quantities are concentrated on the left side, while the known quantities at time levels t and $t+\Delta t/2$ on the right side are:

$$\hat{\omega} = \left[\omega^t - \Delta t_- W^0 \Delta\phi^t + \Delta t_- a_\omega^{t+\Delta t/2}\right]_* + \Delta t_+ a_\omega^{t+\Delta t/2} \ , \tag{3.6a}$$

$$\tilde{u} = \left[u^t - \Delta t_- \overline{\nabla}_x \left(\varphi^0 + \phi\right)^t + \Delta t_- {a_u}^{t+\Delta t/2}\right]_* + \Delta t_+ {a_u}^{t+\Delta t/2}, \tag{3.6b}$$

$$\tilde{v} = \left[v^t - \Delta t_- \overline{\nabla}_y \left(\varphi^0 + \phi\right)^t + \Delta t_- {a_v}^{t+\Delta t/2}\right]_* + \Delta t_+ {a_v}^{t+\Delta t/2}, \tag{3.6c}$$

$$\hat{T} = \left[T'^t + \Delta t_- \left(S^0(\overline{\omega}^\eta)^t + a_T^{t+\Delta t/2}\right)\right]_* + \Delta t_+ a_T^{t+\Delta t/2} \ , \tag{3.6d}$$

$$\tilde{\chi} = \sum_{k=1}^{klev} \left\{ \left[\Delta_k B\chi^t - \Delta t_- \left(\frac{\Delta_k p^0}{p_s^0}(D_k^0)^t + a_{\chi k}^{t+\Delta t/2}\right)\right]_{*2D} - \Delta t_+ a_{\chi k}^{t+\Delta t/2} \right\}, \tag{3.6e}$$

$$\hat{\mathcal{D}} = \frac{1-\varepsilon}{1+\varepsilon}\left(D^0 + \frac{\Delta\omega}{\Delta p^0}\right)_*^t + \frac{1-\varepsilon}{1+\varepsilon}(a_D)_*^{t+\Delta t/2} + (a_D)^{t+\Delta t/2}. \tag{3.6f}$$

As an intermediate notation we use here $\tilde{u}, \tilde{v}.\tilde{\chi}$, the final quantities $\hat{u}, \hat{v}, \hat{\chi}$ arrive after some further modification a while later.

The subscript '$*$' at the brackets means that the quantity in brackets is evaluated in the departure point $\mathbf{x}_{*ijk}^t$, corresponding to the final grid-point under consideration $\mathbf{x}_{ijk}^{t+\Delta t}$, whereas subscript '$*2D$' means that that the corresponding expression in the brackets is evaluated in the location of departure point projection onto kth η-level.

The velocities ω and $m\dot{\eta}$, required at time levels t ja $t+\Delta t/2$ in several a-terms in (3.6), are diagnosed in correspondence with formulae (2.5) – (2.7).

4 Disclosure

To get prognostic quantities explicitly, the system (3.6) has to be solved with respect to $\omega^{t+\Delta t}$, $\mathbf{v}^{t+\Delta t}$, $(T')^{t+\Delta t}$, and $\phi^{t+\Delta t}$. For that we first express quantities $\omega^{t+\Delta t}$, $\mathbf{v}^{t+\Delta t}$, $(T')^{t+\Delta t}$, $(\varphi^0)^{t+\Delta t}$ and $\phi^{t+\Delta t}$ via a new auxiliary potential ξ using equations (3.6a) – (3.6e), and then apply equation (3.6f) to get an elliptic equation for diagnosis of ξ.

4.1 Reduction of prognostic quantities to the auxiliary potential ξ

The aim is to express all prognostic quantities via a new auxiliary potential ξ. The task consists of four steps.

(1) Expression of $(\varphi^0+\phi)^{t+\Delta t}$ via auxiliary potential ξ and $\chi^{t+\Delta t}$.
Considering (3.1) on time level $t+\Delta t$, and using formulae (5) and (7) yields equation for $\phi+\varphi^0$

$$i,j,k: \qquad (\phi+\varphi^0)^{t+\Delta t} = Q + C^2\chi^{t+\Delta t} + \xi \tag{4.1}$$

(note that $\chi=\chi_{ij}$ is independent of height index k), where

$$i,j,k: \qquad Q = R^0\hat{\Gamma}^0\left(\hat{T}+\Delta t_+ S^0\overline{\hat{\omega}}^{\eta}\right)\ , \tag{4.2}$$

$C=\sqrt{R^0T^0(p_s^0)}$ is the isochoric sound speed in reference state, and ξ is an auxiliary potential

$$i,j,k: \qquad \xi = \phi^{t+\Delta t} - (\Delta t_+)^2 R^0\hat{\Gamma}^0(S^0\overline{W^0\Delta\phi^{t+\Delta t}}^{\eta}). \tag{4.3}$$

From this definition, a recurrence follows for every fixed pair of indexes *i,j*:

$$\Delta_{k+1/2}\xi = \Delta_{k+1/2}\phi^{t+\Delta t} + (\Delta t_+)^2 R^0\overline{\alpha^0 S^0\overline{W^0\Delta\phi^{t+\Delta t}}^{\eta}}^{\eta}_{k+1/2}, \tag{4.4}$$

which is convenient to use for transition from ϕ to ξ and vice versa. The boundary condition for ξ proceeds from (4.3) as

$$\overline{\xi}^{\eta}_{klev+1/2} = \overline{\phi}^{\eta}_{klev+1/2} = 0. \tag{4.5}$$

The presentation holds

$$R^0\overline{\alpha^0 S^0\overline{W^0\Delta\phi^{t+\Delta t}}^{\eta}}^{\eta}_{k+1/2} = N^2_{k+1/2}\Delta_{k+1/2}\phi^{t+\Delta t} + \mathcal{O}_2(\Delta\phi^{t+\Delta t})$$

where

$$N^2_{k+1/2} = R^0 W^0_{k+1/2}\overline{\alpha^0 S^0}^{\eta}_{k+1/2} \tag{4.6}$$

is the squared Brent-Väisälä frequency of the reference state on levek $k+1/2$ and

$$\mathcal{O}_2(\Delta\phi^{t+\Delta t}) = \frac{R^0}{4}\Delta\left[\alpha^0 S^0\Delta\left(W^0\Delta\phi^{t+\Delta t}\right)\right].$$

This term can be estimated as $\mathcal{O}_2(\Delta\phi^{t+\Delta t}) \sim \Delta^2(N^2\Delta\phi) \sim (\Delta\eta)^2|N^2\Delta\phi|$ and thus, it tends to zero with the level number increase like $1/klev^2$ (because $\Delta\eta \sim 1/klev$). In a 30–level model its relative value with repsect to the first term is $\sim 10^{-3}$, and $\sim 10^{-4}$ in a 100–level model. Thus, term $\mathcal{O}_2(\Delta\phi^{t+\Delta t})$ can be omitted, after which (4.4) becomes

$$i,j,k{+}1/2: \qquad \Delta\xi = (1+\Delta t_+^2 N^2)\Delta\phi^{t+\Delta t} \tag{4.7}$$

(where $N^2_{k+1/2}$ does not depend on horizontal indexes *i,j*).

(2) Expression of horizontal wind via χ and ξ.

Using (4.1), horizontal wind equations (3.5b), (3.5c) can be modified to

$$i{+}1/2,j,k: \qquad u^{t+\Delta t} = \hat{u} - \Delta t_+ \overline{\nabla}_x \left(C^2\chi+\xi\right)^{t+\Delta t} \ , \tag{4.8a}$$

$$i,j{+}1/2,k: \qquad v^{t+\Delta t} = \hat{v} - \Delta t_+ \overline{\nabla}_y \left(C^2\chi+\xi\right)^{t+\Delta t} \ , \tag{4.8b}$$

$$\hat{u} = \tilde{u} - \overline{\nabla}_x Q, \quad \hat{v} = \tilde{v} - \overline{\nabla}_y Q, \tag{4.8c}$$

Applying of $\overline{\nabla}\cdot$ to (4.8) yields expression for 2D divergence (horizontal wind divergence)

$$i,j,k: \qquad (D^0)^{t+\Delta t} = (\overline{\nabla}_x\hat{u} + \overline{\nabla}_y\hat{v}) - \Delta t_+ \overline{\nabla}^2 \left(C^2\chi+\xi\right)^{t+\Delta t} \ . \tag{4.9}$$

(3) Expression of logarithmic pressure fluctuation χ via auxiliary potential ξ.

Substitution (4.9) into (3.5e) yields after some algebra

$$i,j: \qquad \chi^{t+\Delta t} - \mathcal{H}\xi^{t+\Delta t} = \hat{\chi}, \tag{4.10a}$$

$$\mathcal{H}\xi^{t+\Delta t} = \Delta t_+^2 \frac{\overline{\nabla}^2}{1-\Delta t_+^2 C^2 \overline{\nabla}^2} \sum_{k=1}^{klev} \frac{\Delta p_k^0}{p_s^0} \xi_k^{t+\Delta t}, \tag{4.10b}$$

$$\hat{\chi} = \frac{1}{1-\Delta t_+^2 C^2 \overline{\nabla}^2} \left(\tilde{\chi} - \Delta t_+ \sum_{k=1}^{klev} \frac{\Delta p_k^0}{p_s^0} (\overline{\nabla}_x\hat{u} + \overline{\nabla}_y\hat{v})_k \right), \tag{4.10c}$$

(4) Equation for ξ.

As now $\chi^{t+\Delta t}$ is expressed via ξ with the help of (4.10a), prognoses of vertical wind (3.5a), temperature (3.5d), and horizontal wind (4.8) include still just one unknown variable ξ. To find this auxiliary potential, we apply continuity condition (3.5f). Substitution of wind components (3.5a), (4.8) into (3.5f), and using (4.7) gives the following Laplace equation for ξ

$i,j,k:$
$$(\mathcal{L}+\overline{\nabla}^2)\xi = -C^2\overline{\nabla}^2\chi + \mathcal{D}\ ,$$

where

$$(\mathcal{L}\xi) = \frac{1}{\Delta p^0}\Delta\left(\frac{W^0}{1+\Delta t_+^2 N^2}\Delta\xi\right)\ ,$$

$$\mathcal{D} = \frac{1}{\Delta t_+}\left(\hat{\mathcal{D}} + \overline{\nabla}_x\hat{u} + \overline{\nabla}_y\hat{v} + \frac{\Delta\hat{\omega}}{\Delta p^0}\right)\ .$$

As the right side includes χ, this equation must be treated simultaneously with (4.10a).

Solution method is rather analogous with those, applied in the Eulerian cases (Männik and Rõõm 2001, Rõõm and Männik 2002). Major difference is the lower boundary condition, which is the homogeneous Dirichlet' condition (4.5) in the present case. To take the lower BC into consideration, we add a singular boundary source at the lower boundary, $\gamma\delta_{klev+1,k}$, to the right side of the Laplace equation[5]. Thus, the elliptic system is finally

$i,j:$
$$\left[\mathcal{L}\xi + \overline{\nabla}^2\xi\right]_k = \mathcal{D}_k - C^2\overline{\nabla}^2\chi + \gamma\delta_{klev+1,k}\ , \qquad (4.11a)$$

$i,j:$
$$(\mathcal{B}\xi) \equiv \overline{\xi}^{\eta}_{klev+1/2} = 0, \qquad (4.11b)$$

$i,j:$
$$\chi - (\mathcal{H}\xi) = \hat{\chi}, \qquad (4.11c)$$

This set of equations has to be solved with respect to unknowns ξ_{ijk}, χ_{ij}, and γ_{ij}.

[5]Actually, the singular boundary source is not obligatory. The same special solution can be described by a solution of homogeneous equation. However, singular source introduction allows for application of the same inversion algorithm for all components of the complete solution.

4.2 Solution of the elliptic system

As $\overline{\nabla}^2$ is horizontally homogeneous, i.e. it has constant grid-steps in both directions, the 2D discrete Fourier transformation of system (4.11) will be advantageous. Using for spectral transforms of ξ, χ, γ notation $\tilde{\xi}_{ijk}$, $\tilde{\chi}_{ij}$, $\tilde{\gamma}_{ij}$, for each pair of spectral numbers i, j we get an independent system

$$i,j: \qquad (\mathcal{L}_k - \Lambda)\,\tilde{\xi} = \tilde{\mathcal{D}}_k + C^2\Lambda\tilde{\chi} + \tilde{\gamma}\delta_{klev+1,k}\ , \tag{4.12a}$$

$$i,j: \qquad (\mathcal{B}\tilde{\xi}) \equiv \tilde{\bar{\xi}}^{\eta}_{klev+1/2} = 0, \tag{4.12b}$$

$$i,j: \qquad \tilde{\chi} - (\mathcal{H}\tilde{\xi}) = \tilde{\hat{\chi}}, \tag{4.12c}$$

where $\tilde{\mathcal{D}}_k \equiv \tilde{\mathcal{D}}_{ijk}$ and $\tilde{\hat{\chi}} \equiv \tilde{\hat{\chi}}_{ij}$ are the spectral transforms of sources $\mathcal{D}$ and χ,

$$\Lambda_{ij} = \frac{4}{\langle\Delta x\rangle^2}\sin^2\left(\frac{\pi}{2}\frac{i-1}{klon-1}\right) + \frac{4}{\langle\Delta y\rangle^2}\sin^2\left(\frac{\pi}{2}\frac{j-1}{klat-1}\right),$$

is the Fourier presentation of $-\overline{\nabla}^2$ with $\langle\Delta x\rangle$, $\langle\Delta y\rangle$ representing the average grid-steps in x- and y-directions.
The solution of (4.12a) is

$$\tilde{\xi}_k = \xi^D_k + \tilde{\chi}_k\xi^{\chi}_k + \tilde{\gamma}_{ij}\xi^{\gamma}_k, \tag{4.13a}$$

where ξ^D_k, ξ^{χ}_k, ξ^{γ}_k are solutions of eq. (4.12a) for respective right-hand sources $\tilde{\mathcal{D}}_k$, $C^2\Lambda$ and $\delta_{klev+1,k}$, i.e., they are solutions of the equations

$$(\mathcal{L}_k - \Lambda)\,\xi^D = \tilde{\mathcal{D}}_k, \qquad (\mathcal{L}_k - \Lambda)\,\xi^{\chi} = C^2\Lambda, \qquad (\mathcal{L}_k - \Lambda)\,\xi^{\gamma} = \delta_{klev+1,k} \tag{4.13b}$$

respectively. After these solutions are specified, the substitution of (4.13a) into conditions (4.12b), (4.12c) results in a two-dimensional linear system for $\tilde{\chi}_{ij}$ and $\tilde{\gamma}_{ij}$

$$i,j: \qquad \tilde{\chi}(\mathcal{B}\xi^{\chi}) + \tilde{\gamma}(\mathcal{B}\xi^{\gamma}) = -\mathcal{B}\xi^D, \tag{4.14a}$$

$$i,j: \qquad \tilde{\chi}(1 - \mathcal{H}\xi^{\chi}) - \tilde{\gamma}(\mathcal{H}\xi^{\gamma}) = \hat{\chi} + \mathcal{H}\xi^D. \tag{4.14b}$$

Solution of this linear set accomplishes the solution of the elliptic system and altogether it does accomplish the whole time-stepping procedure.

For intermediate calculations, the nonhydrostatic geopotential ϕ is required, for which a recurrence, resulting from (4.7), can be used:

$$\phi_k = \phi_{k+1} + \frac{\xi_k - \xi_{k+1}}{1 + \Delta t_+^2 N_{k+1/2}^2},$$

with initial value

$$\phi_{klev} = \frac{\xi_{klev}}{1 + \Delta t_+^2 N_{klev+1/2}^2},$$

following from boundary condition (4.5).

For solution of equations (4.13a), the elementary Gaussian elimination method is applied, instead of previous, more sophisticated eigenvector (normal mode) approach, used in Eulerian case (Männik and Rõõm 2001, Rõõm and Männik 2002) [6].

[6]However, the eigenvector approach has its value and may be needed in future, when the domain of integration is chosen/becomes such large (area size 5000 km or larger), that the curvature of the domain cannot be considered as a small perturbation anymore, and, consequently, the Fourier transform in y-direction becomes invalid.

5 Numerical tests

The nonhydrostatic semi-implicit semi-Lagrangian scheme, described in the previous sections, is realized numerically as the extension of the hydrostatic HIRLAM. The departure-point calculation algorithms of HS SISL are maintained completely. The pre- and post-processing facilities are also completely those of the hydrostatic HIRLAM, and the lateral boundary treatment is the same as well (the Davies' boundary relaxation scheme). The numerical code includes all the previous stuff: hydrostatic Eulerian explicit scheme, Eulerian semi-implicit scheme, Lagrangian semi-implicit scheme, and Eulerian NH explicit and semi-implicit sub-models, included as options which may be switched on/off . The numerical code has a parallel realization on the Linux-clusters (Tartu Observatory cluster, EMHI facility, and the Tartu University Environmental Institute's cluster, all in Estonia). In principle, the numerical code should work on all architectures which are supported by HIRLAM. In the following, some provisional results are presented, the purpose of which is to demonstrate the computational efficiency and precision characteristics of the NH SISL model. All results are obtained with NH SISL version which has been ported to official HIRLAM release 6.4.0.

5.1 Flow over artificial orography

Aim of the model experiments is (1) debugging, and (2) model quality control. In these experiments adiabatic stationary flow regimes over given orography are studied and compared to the known analytical solutions of the linearised dynamics. The first test experiment contains a high-resolution adiabatic simulation with artificial orography and an artificial initial state which, however, is quite close to the reality. For orography, as usual, a 'Witch of Agnesi'-type isolated hill serves with the orography function

$$h(x,y) = \frac{h_0}{[1+(x/a_x)^2+(y/a_y)^2]^s} \ , \tag{4.1}$$

where h_0 is the mountain height and $a_x,\ a_y$ are the half-widths of the hill along coordinate axes. We use $s = 1.5$ when examining flow over an isolated mountain and $s = 1$ when looking at one dimensional flow with $a_y = \infty$.

The initial state is characterized with the reference temperature $T^0(p)$, and wind $U(p)$, which is initially taken independent of x, y coordinates and then

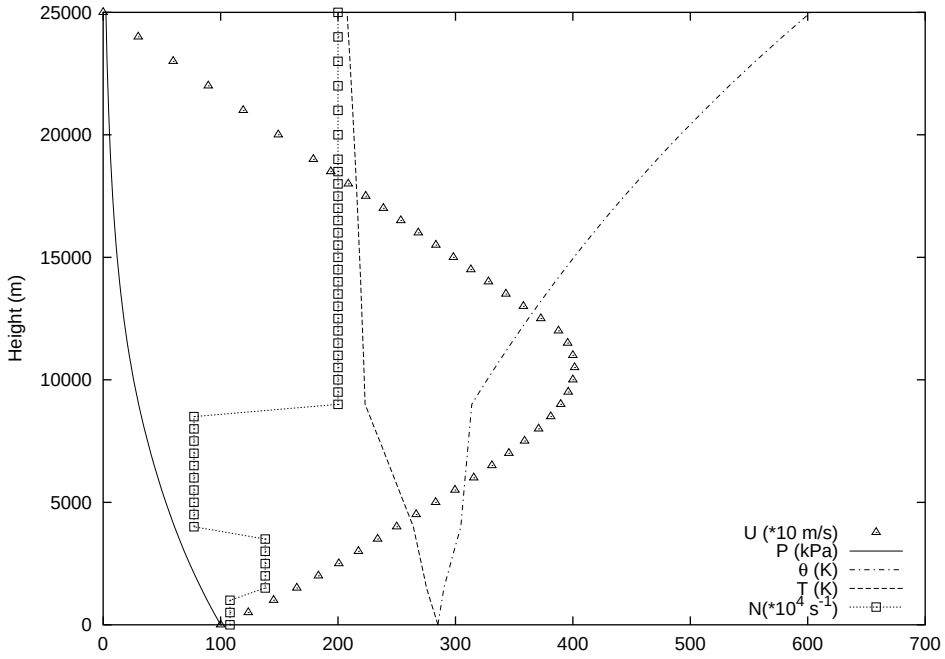

Figure 1: Vertical profiles of wind U, pressure p, potential temperature Θ, temperature T, and Brunt-Väisäla frequency N in the experiment with artificial orography.

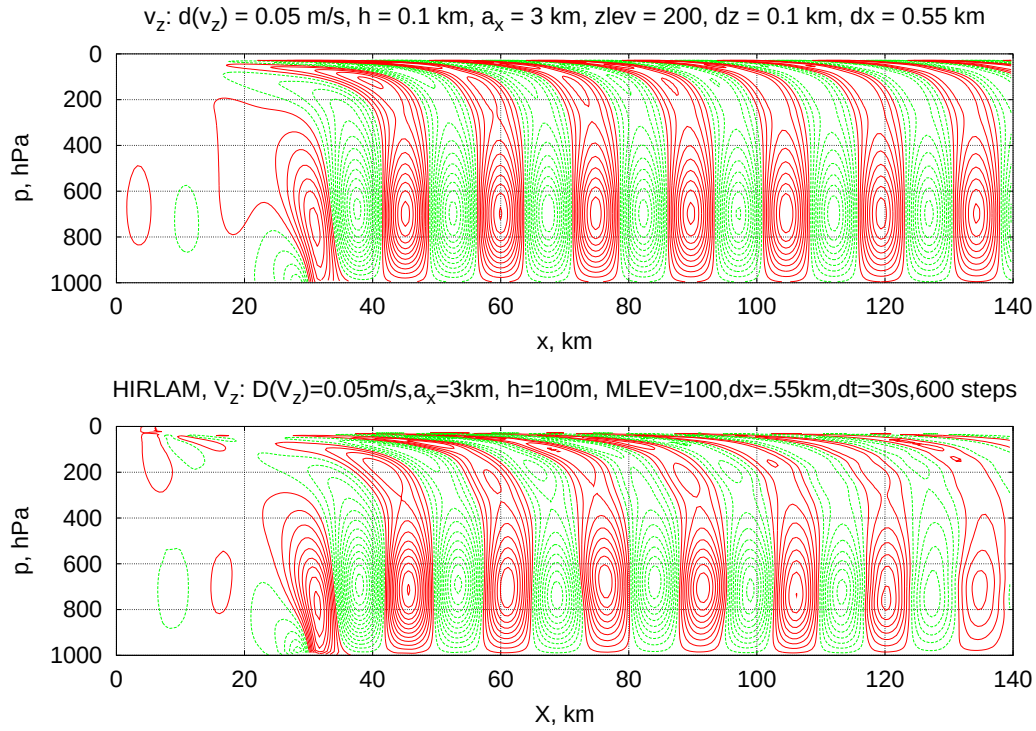

Figure 2: Vertical velocity waves (isoline interval 0.05 m/s) at stationary flow over Agnesi ridge. Top: linear model, bottom: 5 h forecast with NH SISL, $\Delta t = 30$ s.

transformed to the mass-balanced wind (see formulae (6.1.1) - (6.1.3) in Part II). The reference surface pressure field $\hat{p}_s$ is specified from orography $h(x, y)$, using the barometric formula (2.2) with constant temperature $T(z) = T^0(p_s^0)$. The Coriolis force is zero in this experiment ($f = 0$). Boundary conditions are presented by the boundary fields, which coincide with the background fields: $u_b = U(p)$, $v_b = 0$, $T_b = T^0(p)$. The wind and temperature profiles are relatively complicated and can be seen in Figure 1.

As an example, in Fig. 2 the stationary flow over Agnesi ridge with half-width $a_x = 3$ km and maximum height $h = 100$ m is presented. This mountain is sufficiently low to assume linearity of the flow. The grid is 276x100x100 points, horizontal resolution is 0.55 km. At such a reference state, the waves present a stationary wave-train downstream of the mountain, each wave vertically directed and penetrating the whole depth of the atmosphere. It is

rather difficult to model this wave pattern correctly and the simulation quality is a good indicator of the quality of the numerical scheme. Shown are vertical velocity waves generated by the ridge. The upper panel represents the output of 2D linear, frictionless stationary model and the lower panel is the output of NH SISL. The interval between isolines is 0.05 m/s. As seen from Figure 2, NH SISL can qualitatively represent the wave structure generated by flow over obstacle rather well. However, a small phase error in updraft-downdraft zone location is visible. In addition, the amplitude of the waves is slightly too strong near the obstacle and damped downstream. Most of such behaviour is possibly linked to boundary zone interaction with flow fields. It should be noted that the presented model situation is nonhydrostatic by its nature. HS model is not capable to simulate such down-stream wave-traines at all.

5.2 Real-condition experiments

Following section presents several experiments with real observational initial and boundary data. The output of NH SISL is compared to HS SISL results as reference model. HS SISL has been widely used in operational environments and can be considered as well-tested model. Similarity of the results with HS model offers high degree of reliability and is here regarded as quality measure. The specific additional nonhydrostatic and high resolution effects require deeper studying and much more sophisticated verification methodologies and are left for further research.

The NH SISL adiabatic core was investigated in two cases: In mountainous region with resolution 5.5 km and in lowland conditions with resolution 3.3 km. Additionally, operational performance was evaluated in a two week continuous run experiment.

5.2.1 Norwegian experiment (mountains)

An arbitrarily chosen weather situation with forecast initial time at 00 GMT 5th August 2003 is modelled. The resolution of the model domain is 5.5 km, grid size is 156x156 points, 31 levels. The physics is switched on. Forecast period is 24 h, and the time step is 4 minutes. Analysis files from FMI operational forecast model are used as initial and boundary fields.

The results of the modelling experiments are presented on Figures 3 - 5. The

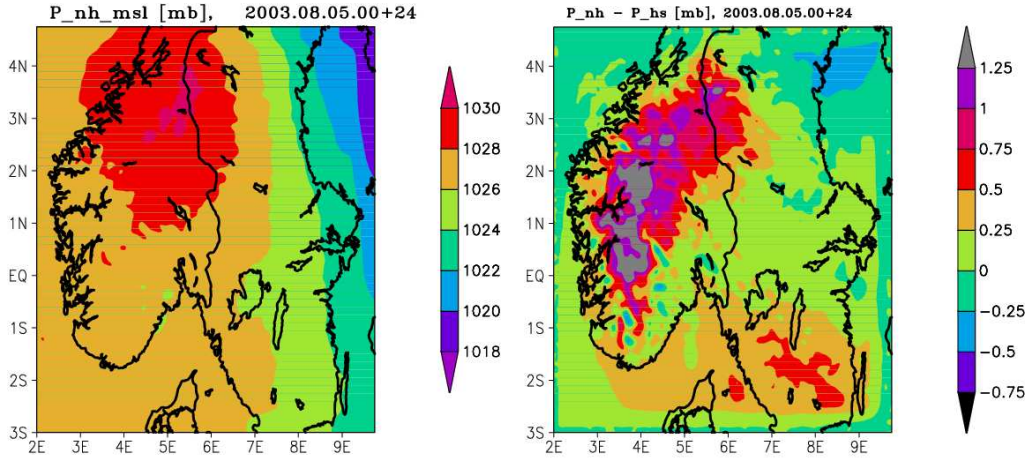

Figure 3: Mean sea-level surface pressure in 24 h Norwegian forecast at 5.5 km resolution with 4 minute time-step. Left: Mean sea level pressure; right: Surface pressure difference from the HS SISL results

weather situation represents a high pressure system over Scandinavia. The performance of the NH SISL over mountainous area (Norwegian mountains) is evaluated. The left panel of the Figure 3 shows pressure reduced to mean sea level of the NH SISL forecast and the difference from HS SISL is on the right panel. As Figure 3 demonstrates, the surface pressure of NH model is approximately 1 mb higher over the mountains.

The forecasted lowest level temperature (Figure 4) does not differ from HS SISL results more than $\pm$ 1.0 K in average. However, scattered spots of small areas, where the temperature differences reach 3 K, do exist. Figure 5 depicts cross-section of U_x component of the wind taken in south-north direction at 6.0E longitude (HIRLAM rotated coordinates). In general, the differences of NH and HS models are small with the exception of a small region in the boundary layer near model equator where the difference reaches almost 10 m/s. This large wind difference is caused by a small-scale yet relatively strong wind gust in this site, which is present in HS model but lacks in the NH case.

It is possible conclude from Figures 3 - 5 that generally NH and HS model produce similar forecasts though local small-scale differences can appear in some areas, caused mainly by slightly different disposing of local fronts (regions with steep change) of meteorological fields by HS and NH models. This means that NH SISL could be used as a forecast model without problems,

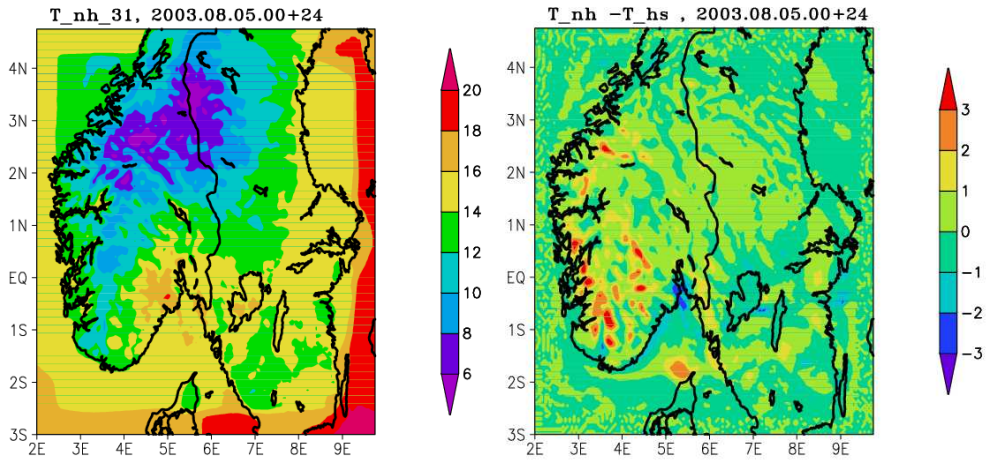

Figure 4: Lowest level temperature in 24 h Norwegian forecast at 5.5 km resolution with 4 minute time-step. Left: Temperature; right: Temperature difference from the HS SISL results

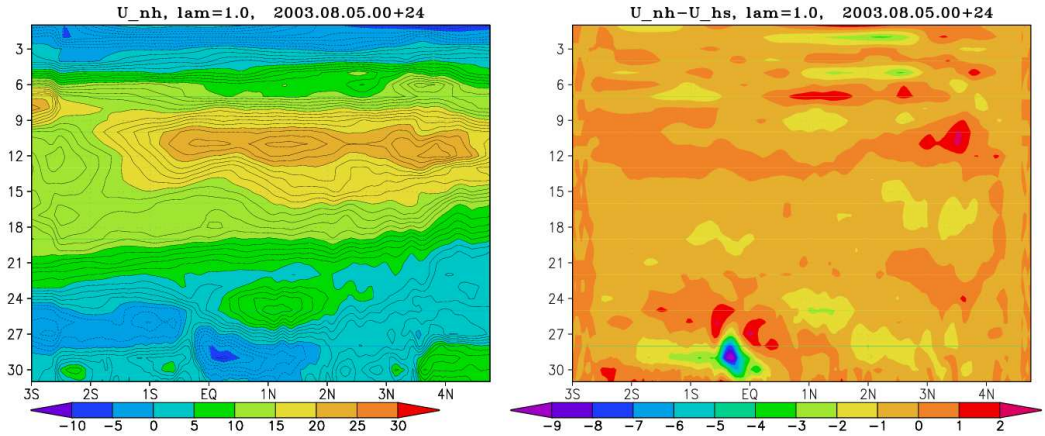

Figure 5: Vertical cross-section of the wind component U_x in 24 h Norwegian forecast at 5.5 km resolution with 4 minute time-step. Left: Vertical cross-section of U_x; right: Departure of U_x from the corresponding HS SISL wind

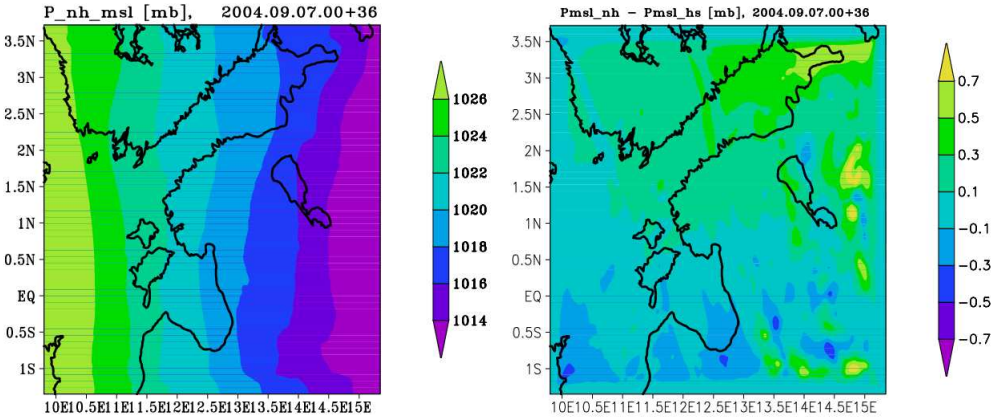

Figure 6: Surface pressure in 36 h Estonian B-area forecast at 3.3 km resolution with 2.5 minute time-step. Left: Sea level pressure. Right: Surface pressure difference from the HS SISL results.

but local effects and differences from HS model, most probably resulting from different interaction of HS and NH models with the 'physics', present interest and require additional sudying.

5.2.2 Estonian B-area experiments (lowlands)

Experiments, similar to the previous case, were carried out over relatively flat area. Reference physics was included. The date was arbitrarily chosen to be 7th September 2004 and a 36h forecast was produced starting from 00 GMT. The area is the 3.3 km resolution modelling domain used at EMHI-s experimental high resolution NWP environment – so called Estonian B-area (ETB). The grid in this case is 186×170 points, 40 levels in vertical. It is worth mentioning that the former Eulerian SI model based domain grid was 104×100 points. Thus, the increase in the forecast area due to implementation of more efficient NH SISL scheme is about 3.3 times (1.7 times in each horizontal direction). The time-step in this experiment was 2.5 min (150 s).

In Figure 6 and 7, the 36 h MSL surface pressure and lowest level temperature are presented. Left panels show NH SISL forecast and right panels represent differences from HS SISL forecast. The differences with the HS SISL model do not exceed in the current lowland case ± 0.7 mb in surface pressure, and

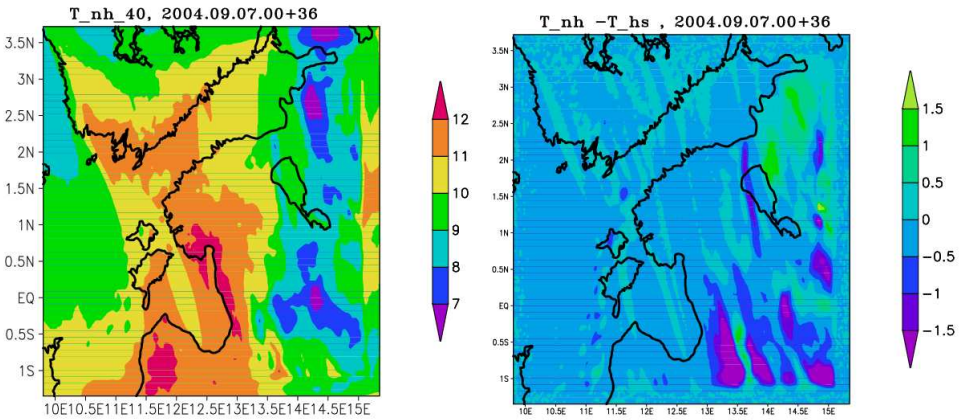

Figure 7: Lowest level temperature T_{40} in 36 h Estonian B-area forecast at 3.3 km resolution with 2.5 minute time-step. Left: Temperature. Right: Temperature difference from the HS SISL results.

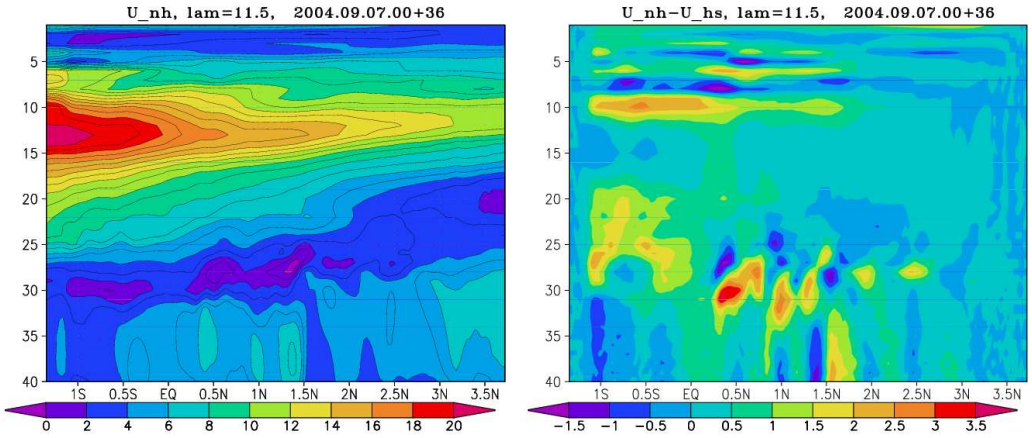

Figure 8: Vertical cross-section of the wind component U_x in 36 h Estonian B-area forecast at 3.3 km resolution with 2.5 minute time-step. Left: Vertical cross-section of U_x; Right: Departure of U_x from the corresponding HS SISL wind.

$\pm 1.5\ ^{o}$ C in the lowest level temperature fields. Figure 8 shows the cross-section of the u-component of the wind of 36 hour forecast and its difference from HS model run. The cross section is taken along 11.5E meridian. In general the flow fields are very similar in structure. The differences between two models reach 2 m/s.

On large scale, the NH SISL and HS SISL models give similar results like in the previous model experiment. The differences between them are local, although clearly observable. The regions of differences are small-sized, relatively sporadic and difficult to verify against the real situation.

In general, the overall quality of NH SISL looks satisfactory and its performance can be considered reliable.

5.2.3 Comparison with observations

A two week long modelling experiment was carried out to obtain quantitative measures of NH SISL performance in comparison with the observations. The modelling domain in the experiment was the hereinabove described ETB area. Integration time the was 150 s. The selected time period was from January 01 to January 14, 2005. High cyclonic activity was observed in the area during the period and it included also the devastating storm on 8th January. The standard verifications scores against observations were used. To get a reference information, the same verification statistics were collected from HS SISL on the same area and from HS SISL with 11 km resolution. To be able to compare the models with different areas and resolutions, a specific set of observational sites was chosen containing all WMO sites in the ETB area. The quality of observational sites in the list was not critically evaluated.

The results are presented in Figures 9 and 10. In Figure 9, the verification statistics for sea-level pressure, 2 m temperature, 10 m wind and 2m relative humidity of all three models are presented. Both high resolution models give similar performance with the exception of mean sea level pressure statistics. The mean sea level pressure bias of NH SISL is slightly better during early forecast and worse at longer forecast times. High resolution models improve the 10 m wind errors and 2m relative humidity biases, while the low resolution HS model tend to have better 2m temperature scores and 2 m relative humidity root mean square errors. Possible explanation is that the better wind forecast from high resolution models results from better resolution of

orography, while the better temperature forecast of the lower resolution HS model results from better tuning of various physical parameterizations. Figure 10 shows verification scores of 36h forecasts of all three models against vertical sounding observations. The differences between all three models exist, but they are not big and it is relatively hard to speculate which model is better.

From the Figures 9 - 10 it is possible to conclude that in the flat lowland case, NH model offers the same forecast quality as its hydrostatic parent does. On the basis of the standard verification scores, there is no remarkable benefit nor from the increased resolution neither from the application of nonhydrostatic scheme. This conclusion is valid for flat areas. The benefits of high resolution and NH treatment become evident, if the wave generation by orography and the orographic drag becomes substantial. Another potential improvement area are the explicitly resolved convective events with strong vertical circulation. However, the convection events need to be investigated on the case by case basis with application of special model verification schemes.

5.3 Computational efficiency

A set of numerical experiments on two different grids were used to analyze the computational resource requirements of NH SISL in comparison with HS SISL. 1-hour forecasts were computed with both schemes on $114 \times 100 \times 40$ and $186 \times 170 \times 40$ grids. The time-step was 400 s for the smaller grid and 150 s for larger grid. The computations were performed on four-node Linux cluster computer which has 3 GHz processors connected with Gigabit Ethernet cards. The results are presented in Table 1.

Table 1.

Grid	HS SISL comp. time (net processor time/gross time/ratio)	NH SISL comp. time (net processor time/gross time/ratio)	NH / HS ratio
$114 \times 100 \times 40$	15.2/18.6/0.82	23.8/28.4/0.83	1.53
$186 \times 170 \times 40$	84.3/99.6/0.85	119.6/144.1/0.83	1.45

In the table net processor time refers to the computing time spent on processors measured by HIRLAM routines. Gross time refers to the time, spent

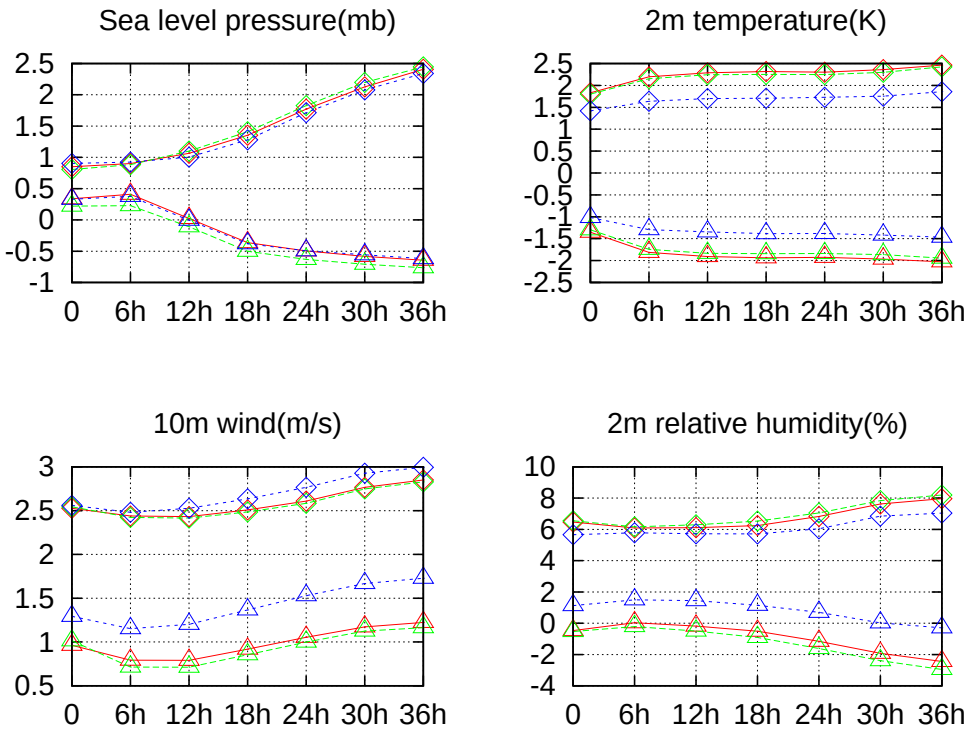

Figure 9: RMS errors (rhomb) and biases (triangle) for sea-level pressure, 2 m temperature, 10 m wind and 2 m relative humidity at different forecast lengths. Red line marks HS SISL with 3.3 km resolution, green line NH SISL at 3.3 km resolution and blue line HS SISL with 11 km resolution.

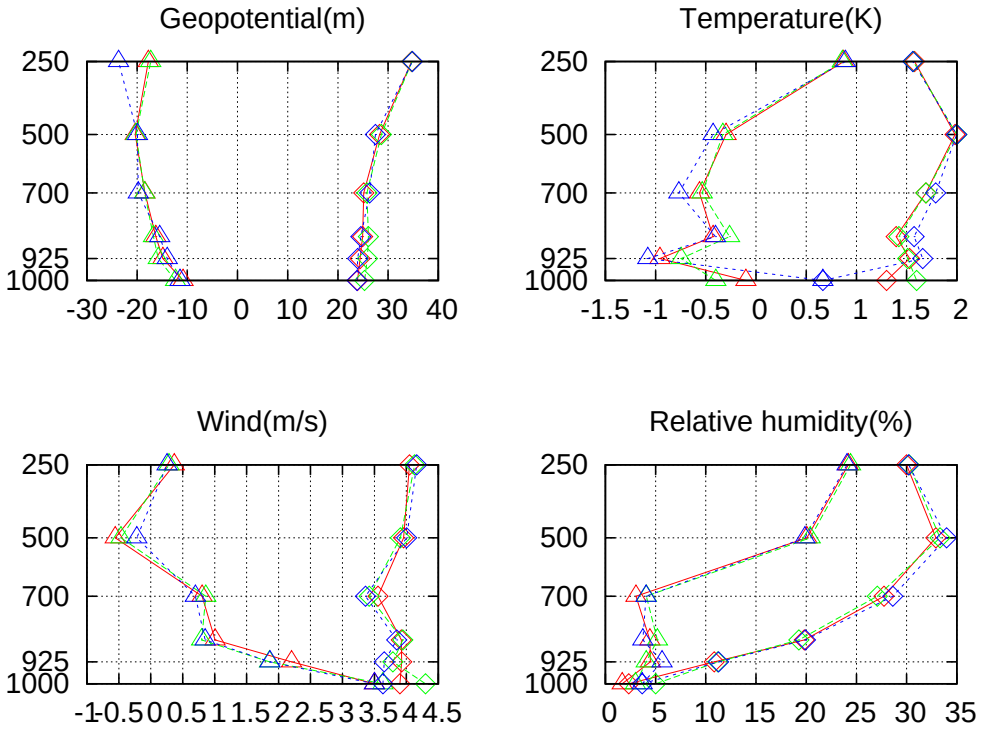

Figure 10: RMS errors (rhomb) and biases (triangle) for geopotential height, temperature, wind and relative humidity of 36 h forecast at different pressure levels. Red line marks HS SISL with 3.3 km resolution, green line NH SISL at 3.3 km resolution and blue line HS SISL with 11 km resolution.

on computing, measured by routinee MPI_Wtime. The difference is caused by the limited communication bandwidth. The table shows that the ratio of computation and communication costs is roughly the same for both schemes. The NH SISL scheme requires 1.5 times more computational resources than HS SISL when the time-step is equal.

It ought to be possible some further increase of efficiency of the NH code by means of code optimization.

6 Conclusions

We consider the NH SISL development as the completed task. The stability and the time step characteristics of the new model are reasonable. Comparison with theoretical results (mountain flows), as well as with HS SISL shows that NH SISL is reliable and ready for applications. The increase of computational efficiency is substantial in comparison with Eulerian case and looks reasonable in comparison with HS SISL in similar conditions.

Currently, the NH SISL is implemented as the adiabatic core in Estonian B-area model (3.3 km resolution, grid 186x170, 40 levels). Since August 2005, the NH SISL code is ported to the latest official HIRLAM reference version 6.4.0, and its preoperational testing is launched at EMHI. As the preliminary statistical testing reveals, the NH-specific effect is moderate at these resolutions for the given physical paramterization and lowlands condition. More NH behaviour will be expected at very high spatial resolutions (0.5 - 1km, 100 levels), in which case NH SISL will be a suitable tool for development and testing of new physics, including the complex terrain, boundary layer, and moist convection.

Acknowledgments

This investigation has been supported by the **Estonian Science Foundation** under grant 5711.

A. Luhamaa is supported by the **Väisälä Foundation** under the auspice of the **Finnish Academy of Sciences**.

Appendix 1

7 Notations

7.1 Physics constants

r_0 - radius of the Earth

g - gravitational acceleration

R^0, c_v^0, c_p^0, $\kappa = R^0/c_p^0$ - dry air constants

R, c_v, c_p - moist air constants

$f = 2\Omega \sin\varphi$ - Coriolis parameter as the function of geographical latitude φ

7.2 Model constants

$T^0(z)$, $T^0(p)$ - reference temperature as a function of height or pressure

$p_s^0 = 1013.26$ hPa - climatological mean sea-level pressure

$C = \sqrt{R^0 T^0}$ - isochoric sound speed

$N, N_{k+1/2}$ - Brunt-Väisälä frequency of reference state

S_k^0 - reference state static stability

7.3 Area, geometry and coordinates

t - time

Δt - time-step $\Delta t^{\pm} = \frac{1\pm\varepsilon}{2}\Delta t$

$\mathbf{k}$ - local vertical unit vector

k - index of full η-level

$k + 1/2$ - index of η half-level

$klev$ - number of discrete η-levels

η - η–coordinate

η_k, $\eta_{k+1/2}$ - full and half η-levels

$klon, klat$ - number of grid-points in x- and y-directions

i, j - indexes of mass-points in x- and y-direction

$i+1/2$ - index of u-point in x-direction
$j+1/2$ - index of v-point in y-direction
$\lambda_i = i\Delta\lambda, \theta_j = j\Delta\theta$ - angular coordinates of a mass-point in rotated spherical coordinates
$h_{xij} = \cos\theta_j$, $h_{yij} = 1$ - stereometrical coefficients for spherical geometry (ECMWF originated HIRLAM notation)
$x_{ij} = r_0 h_{xij}\lambda_i$, $y_{ij} = r_0 h_{yij}\theta_j$ - physical coordinates of a mass-point
$\Delta x_{ij} = r_0 h_{xij}\Delta\lambda$, $\Delta y_{ij} = r_0 h_{yij}\Delta\theta$;

7.4 Operators

$\overline{a}^{\eta}_k = (a_{k-1/2} + a_{k+1/2})/2$, $\overline{a}^{\eta}_{k+1/2} = (a_k + a_{k+1})/2$ - vertical averaging
$\overline{a}^{x}_i = (a_{i-1/2} + a_{i+1/2})/2$, $\overline{a}^{x}_{i+1/2} = (a_i + a_{i+1})/2$ - horizontal averaging in x-direction
$\overline{a}^{y}_j = (a_{j-1/2} + a_{j+1/2})/2$, $\overline{a}^{y}_{j+1/2} = (a_j + a_{j+1})/2$ - horizontal averaging in y-direction
$\langle u\rangle_k = \frac{1}{klonklat}\sum_{ij} u_{ijk}$ - averaging over η-levels with given orography

Vertical difference operatorΔ:
$\Delta_k\varphi = \varphi_{k+1/2} - \varphi_{k-1/2}$, $\Delta_{k+1/2}\xi = \xi_{k+1} - \xi_k$;
Gradient $\nabla a = \mathbf{i}^x\nabla_x a + \mathbf{i}^y\nabla_y a$ and divergence $\nabla\cdot\mathbf{b} = \nabla_x b_x + \nabla_y b_y$:

- In horizontally continuous model:

$$\nabla_x a = \frac{\partial a}{\partial x} = \frac{\partial a}{h_x r_0\partial\lambda}, \qquad \nabla_y a = \frac{\partial a}{\partial y} = \frac{\partial a}{h_y r_0\partial\theta},$$

$$\nabla\cdot\mathbf{b} = \frac{\partial h_y b_x}{h_x h_y r_0\partial\lambda} + \frac{\partial h_x b_y}{h_x h_y r_0\partial\theta},$$

- In horizontally discrete model:

$$(\nabla_x a)_{i+1/2j} = \frac{a_{i+1j} - a_{ij}}{h_{xi+1/2j} r_0\Delta\lambda} , \qquad (\nabla_y a)_{ij+1/2} = \frac{a_{ij+1} - a_{ij}}{h_{yij+1/2} r_0\Delta\theta} .$$

$$(\nabla\cdot\mathbf{a})_{ij} = \frac{(\overline{h_y}^x a_x)_{i+1/2,j} - (\overline{h_y}^x a_x)_{i-1/2,j}}{(h_x h_y)_{ij} r_0\Delta\lambda} + \frac{(\overline{h_x}^y a_y)_{ij+1/2} - (\overline{h_x}^y a_y)_{ij-1/2}}{(h_x h_y)_{ij} r_0\Delta\theta} ,$$

Horizontally averaged discrete gradient, divergence and Laplacian:

$$(\overline{\nabla}_x a)_{i+1/2} = \frac{a_{i+1} - a_i}{\langle \Delta x \rangle}, \qquad (\overline{\nabla}_y a)_{j+1/2} = \frac{a_{j+1} - a_j}{\langle \Delta y \rangle},$$

$$(\overline{\nabla} \cdot \mathbf{b})_{ij} = \frac{b_{xi+1/2,j} - b_{xi-1/2,j}}{\langle \Delta x \rangle} + \frac{b_{yi,j+1/2} - b_{yi,j-1/2}}{\langle \Delta y \rangle},$$

$$(\overline{\nabla}^2 a)_{ij} = \frac{a_{i+1,j} + a_{i-1,j} - a_{ij}}{\langle \Delta x \rangle^2} + \frac{a_{i,j+1} + a_{i,j-1} - a_{ij}}{\langle \Delta y \rangle^2}.$$

Isobaric gradient and divergence in η-coordinate presentation:

- In continuous case:

$$\hat{\mathbf{G}} = \hat{\mathbf{G}}^+ = \nabla - \frac{\nabla p}{m} \frac{\partial}{\partial \eta}$$

- In horizontally continuous, vertically discrete model:

$$\hat{\mathbf{G}}_k \varphi = \nabla \varphi_k - \frac{1}{\Delta p_k} \overline{\nabla p \Delta \varphi_k}^{\eta}$$

$$\hat{\mathbf{G}}_k^+ \cdot \mathbf{v} = \nabla \cdot \mathbf{v}_k - \frac{1}{\Delta p_k} \overline{\nabla p \cdot \Delta \mathbf{v}_k}^{\eta}$$

- In 3D discrete model

$$(\hat{G}_x \phi)_{i+1/2jk} = \frac{1}{\overline{h_x}^x} \left[\delta_x \phi - \frac{\overline{(\delta_x p) \Delta_\eta \overline{\phi}^x}^\eta}{\overline{\Delta_\eta p}^x} \right]_{i+1/2jk},$$

$$(\hat{G}_y \phi)_{ij+1/2k} = \frac{1}{\overline{h_y}^y} \left[\delta_y \phi - \frac{\overline{(\delta_y p) \Delta_\eta \overline{\phi}^y}^\eta}{\overline{\Delta_\eta p}^y} \right]_{ij+1/2k}.$$

$$(\hat{\mathbf{G}}^+ \cdot \mathbf{v})_{ijk} = (\hat{G}_x^+ u + \hat{G}_y^+ v)_{ijk} =$$

$$\frac{1}{(h_x h_y)_{ij}} \left[\delta_x (\overline{h_y}^x u) - \frac{\overline{\overline{h_y}^x (\Delta_\eta u) \delta_x p}^{x\eta}}{\Delta_\eta p} + \delta_y (\overline{h_x}^y v) - \frac{\overline{\overline{h_x}^y (\Delta_\eta v) \delta_y p}^{y\eta}}{\Delta_\eta p} \right]_{ijk},$$

Lagrangian time derivatives:

- continuous 2D:
$$\frac{\mathrm{d}_k^h f}{\mathrm{d}t} = \frac{\partial f}{\partial t} + \mathbf{v}_k \cdot \nabla f,$$
- Discrete 2D:
$$\frac{\mathrm{d}_k^h f}{\mathrm{d}t} = \frac{f(\mathbf{x}_k, t+\Delta t) - f(\mathbf{x}_*, t)}{\Delta t},$$
where $\mathbf{x}_*$ is the projection of departure point, which destination is $\mathbf{x}_k$, onto surface η_k;
- continuous 3D:
$$\frac{\mathrm{d}f}{\mathrm{d}t} = \frac{\partial f}{\partial t} + \mathbf{v} \cdot \nabla f + \dot{\eta}\frac{\partial f}{\partial \eta},$$
Discrete 3D:
$$\frac{\mathrm{d}_k f}{\mathrm{d}t} = \frac{f(\mathbf{x}_k, t+\Delta t) - f(\mathbf{x}_*, t)}{\Delta t},$$
where $\mathbf{x}_*$ is the departure point for $\mathbf{x}_k$.

7.5 Meteorological fields

$A(\eta)$, $B(\eta)$ – coefficients of vertical coordinate $p \leftrightarrow \eta$ transformation
$A_k = A(\eta_k)$, $B_k = B(\eta_k)$
$p(\eta) = A(\eta) + B(\eta)p_s$ - pressure in η-coordinate presentation
$p_k = A_k + B_k p_s$
$p_s^0, p_s(x, y, t)$ -surface pressure
$\hat{p}_s = \exp(-fh/C^2)$ - surface pressure in reference state
$\chi = \ln(p_s/\hat{p}_s)$ - logarithmic pressure fluctuation
$m = \partial p/\partial \eta$ - non-dimensional density of matter in η-coordinates
$\omega = dp/dt$, $\omega_{k+1/2}$ $\omega_{ijk+1/2}$- 'omega-velocity', speed of pressure change in elementary air volume
$\dot{\eta} = d\eta/dt$ - η-velocity
$\mathbf{v}$, $\mathbf{v}_k$, - horizontal wind vector
u, u_k, $u_{i+1/2,jk}$, v, v_k, $v_{ij+1/2,k}$, - components of the horizontal wind vector
$D_k = \nabla\cdot\ \mathbf{v}_k$ - horizontal divergence

T, T_k - temperature

$T' = T - T^0$

Φ - complete geopotential

ϕ - nonhydrostatic geopotential

φ , φ^*, φ^0 hydrostatic geopotential

a_ω, a_v, a_T, a_χ, a_D nonlinear parts of forcing

$\hat{\omega}$, $\hat{\mathbf{v}}$, $\hat{T}$, $\hat{\chi}$ - explicit developments of ω, $\mathbf{v}$, T' and χ at time-level $t + \Delta t$.

$A_\omega, \mathbf{A_v}, A_T$ diabatic and spectral smoothing terms

$\mathcal{D}, \hat{\mathcal{D}}$ – sources in ϕ–equation

References

Männik, A. and R. Rõõm, 2001: Non-hydrostatic adiabatic kernel for HIRLAM. Part II: Anelastic, hybrid-coordinate, explicit-Eulerian model. *HIRLAM Technical Report*, **49**, 54p.

Männik, A., R. Rõõm, A. Luhamaa, 2003: Nonhydrostaic generalization of a pressure-coordinate-based hydrostatic model with implementation in HIRLAM: validation of adiabatic core. *Tellus*, **55A**, 219 – 231.

Manual 1996:
Källén,E., (Ed), 1996: HIRLAM Documentation Manual, System 2.5, Norrköping, 262 p.

Manual 2002:
Undén P., L. Rontu, H. Järvinen, P. Lynch, J. Calvo, G.Cats, J. Cuxart, K.Eerola, C. Fortelius, J. A. Garcia-Moya, C. Jones, G. Lenderlink, A. McDonald, R. McGrath, B. Navascues, N.W. Nielsen, V. Odergaard, E. Rodrigues, M. Rummukainen, R. Rõõm, K. Shattler, B. H. Sass, H. Savijärvi, B. W. Schreur, R. Sigg, H. The, A. Tijm, 2002: HIRLAM-5 Scientific Documentation, *HIRLAM-5 Project, c/o Per Undén SMHI, S-601 76 Norrköping, SWEDEN*, 144 p.

McDonald, A., 1995: The HIRLAM two time level, three dimensional semi-Lagrangian,semi-implicit, limited area, gridpoint model of the primitive equations. HIRLAM Technical Report No. 17. Norrköping, 1995, 25 pp.

McDonald A., J.-E. Haugen, 1992: A two-time-level,three-dimensional, semi-lagrangian, semi-implicit, limited-area gridpoint model of the primitive equations. *Mon. Weather Rev.*, **120,** 2603 - 2621.

McDonald A., J.-E. Haugen, 1993: A two-time-level,three-dimensional, semi-Lagrangian, semi-implicit, limited-area gridpoint model of the primitive equations. Part II: Extension to hybrid vertical coordinates. *Mon. Weather Rev.*, **121,** 2077 – 2087.

McDonald A., 1998: Alternative extrapolations to find the departure point in a 'two time level' semi-Lagrangian integration. HIRLAM Technical Report No 34. Bublisher: HIRLAM 4 Prject, c/o Met Éireann, Glasnevi Hill, Dublin 9, Ireland. 17 pp.

McDonald A., 1999: An examination of alternative extrapolations to find the departure point position in a 'two-time-level' semi-Lagrangian integration. *Mon. Weather Rev.*, **127,** 1985 – 1993.

Ritchie, H., Tanguay, M., 1996: A comparison of spatially averaged Eulerian and Semi-Lagrangian treatments of mountains. *Mon. Weather Rev.*, **124,** 167 – 181.

Ritchie, H. C. Temperton, A. Simmons, M. Hortal, T. Davies, D. Dent, M. Hamrud, 1995: Implementation of the Semi–Lagrangian method in a high–resolution version of the ECMWF forecast model. *Mon. Weather Rev.*, **123,** 489 – 514.

Robert, A. J., 1969: The integration of a spectral model of the atmosphere by the implicit method. *Proc. WMO-IUGG Symposium on NWP*, Tokyo, Japan Meteorological Agency, VII, 19 - 24.

Robert A J, Henderson J, Thurnbull C, 1972: An implicit time integration scheme for baroclinic models of the atmosphere. *Mon. Weather Rev.*, **100,** 329 Ű 335.

Robert, A., T. L. Yee, H. Richie, 1985: A semi-lagrangian and semi-implicit integration scheme for multi-level atmospheric models. *Mon. Weather Rev.*, **113,** 388 – 394.

Robert, A., 1981: A stable numerical integration scheme for the primitive meteorological equations. *Atmos. Ocean*, **19**, 35 – 46.

Robert, A., 1982: A semi-Lagrangian and semi-implicit numerical integration scheme for the primitive meteorologiacal equations. *J. Meteor. Soc. Japan*, **60**, 319 – 325.

Rõõm, R., 2001: Nonhydrostatic adiabatic kernel for HIRLAM. Part I: Fundametals of nonhydrostatic dynamics in pressure-related coordinates. *HIRLAM Technical Report*, **48**, 26p.

Rõõm, R. A. Männik, 1999: Response of different nonhydrostatic, pressure-coordinate models to orographic forcing. *JAS*, **56,**2553 - 2570.

Rõõm, R. A. Männik, 2002: Nonhydrostatic adiabatic kernel for HIRLAM. Part III: Semi-implicit Eulerian scheme. *HIRLAM Technical Report*, **55**, 29p.

Tanguay, M., A. Robert, R. Laprise, 1990: A semi–implicit semi–Lagrangian fully compressible regional model. *Mon. Weather Rev.*, **118,** 1970 – 1980.

Temperton, C., A. Staniforth, 1987: An efficient two-time-level semi-Lagrangian semi-implicit integration scheme. *Q. J. R. Meteorol. Soc.*, **113**, 1025 – 1039.

White, A.A. ,1989: An extended version of nonhydrostatic, pressure coordinate model. *Q. J. R. Meteorol. Soc.*, **115**, 1243 – 1251.